Supplement of Atmos. Chem. Phys., 26, 3339–3356, 2026
https://doi.org/10.5194/acp-26-3339-2026-supplement

Atmospheric Chemistry and Physics
Open Access
EGU

Supplement of

On the nationwide variability of low-level jets prior to warm-season nocturnal rainfall in China revealed by radar wind profilers

Ning Li et al.

Correspondence to: Jianping Guo (jpguocams@gmail.com)

1. Wind kinetic energy and its vertical transport

The evolution of the LLJ prior to rainfall may be caused by the change in kinetic energy of wind (KE) and its transport (Fu et al., 2020), which are calculated as follows:

$$KE=(u^2+v^2)/2 \quad (1)$$

$$TV=-w\frac{\partial KE}{\partial z} \quad (2)$$

where u, v, and w represent the u and v wind components and vertical velocity as measured by the RWP, respectively, TV represents the transport of kinetic energy in the vertical direction, and z is altitude. If TV < 0, the downward momentum transportation occurs.

References

Fu, S. M., Jin, S. L., Shen, W., Li, D. Y., Liu, B., & Sun, J. H. (2020). A kinetic energy budget on the severe wind production that causes a serious state grid failure in Southern Xinjiang China. Atmospheric Science Letters, 21(7), e977

Tables

Table S1 Statistics of the number of LLJ_HR and LLJ_non-HR events during four rainy season phases under different percentile levels of rainfall intensity

Type	Percentile	Phase 1	Phase 2	Phase 3	Phase 4
LLJ_HR	75th	29	26	15	12
	85th	20	15	10	8
	95th	9	8	5	4
LLJ_non-HR	75th	71	69	30	25
	85th	95	103	47	33
	95th	110	112	53	38

Figures

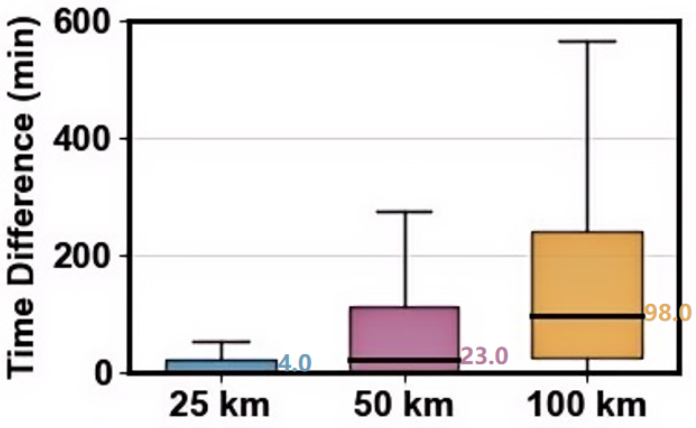

Figure S1. Sensitivity of temporal differences in rainfall event onset to the selection radius. The boxplots display the absolute time difference between the onset of each rainfall event identified by rain gauges within a 25-km, 50-km, or 100-km radius area and the onset of the temporally closest rainfall event identified by the rain gauge co-located with the RWP within four ROIs during corresponding phases.

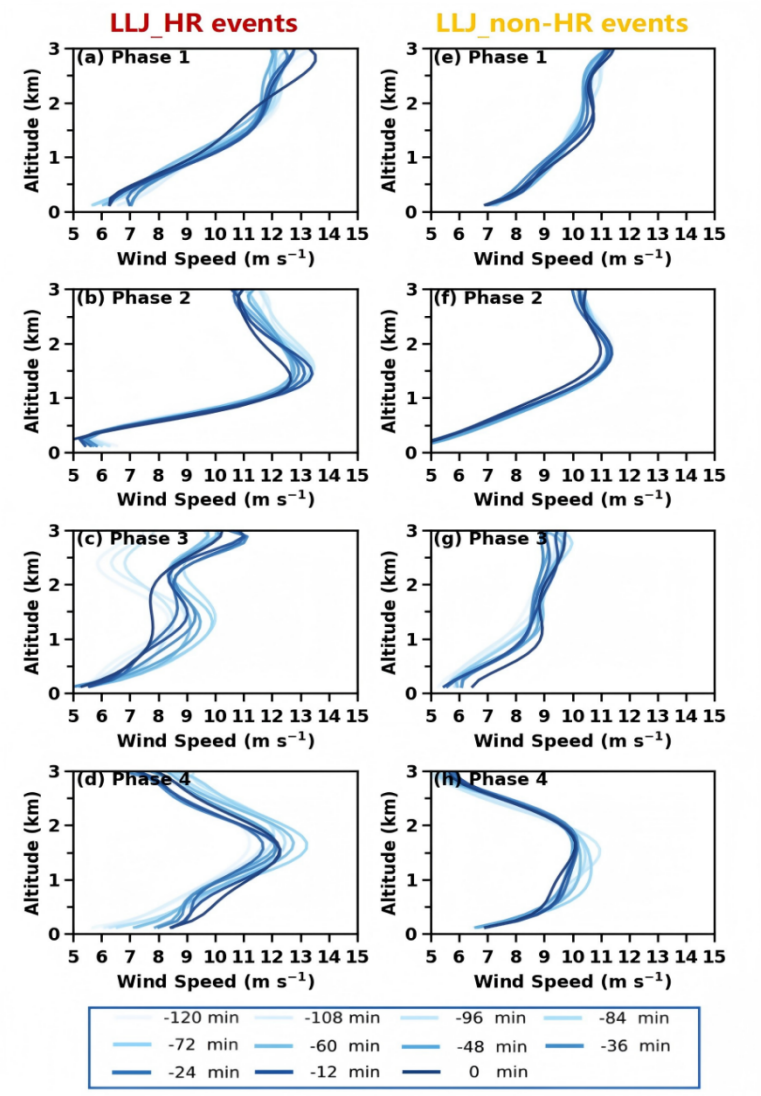

Figure S2. (a-d) Evolution of RWP-detected mean wind profiles of LLJs (blue solid lines, every 12 min) within 2 hours preceding nocturnal rainfall in LLJ-HR events (≥85th percentile) in (a) ROI-1 during Phase 1, (b) ROI-2 during Phase 2, (c) ROI-3 during Phase 3, and (d) in ROI-4 during Phase 4. (e-h) Same as (a-d), but for LLJ_non-HR events

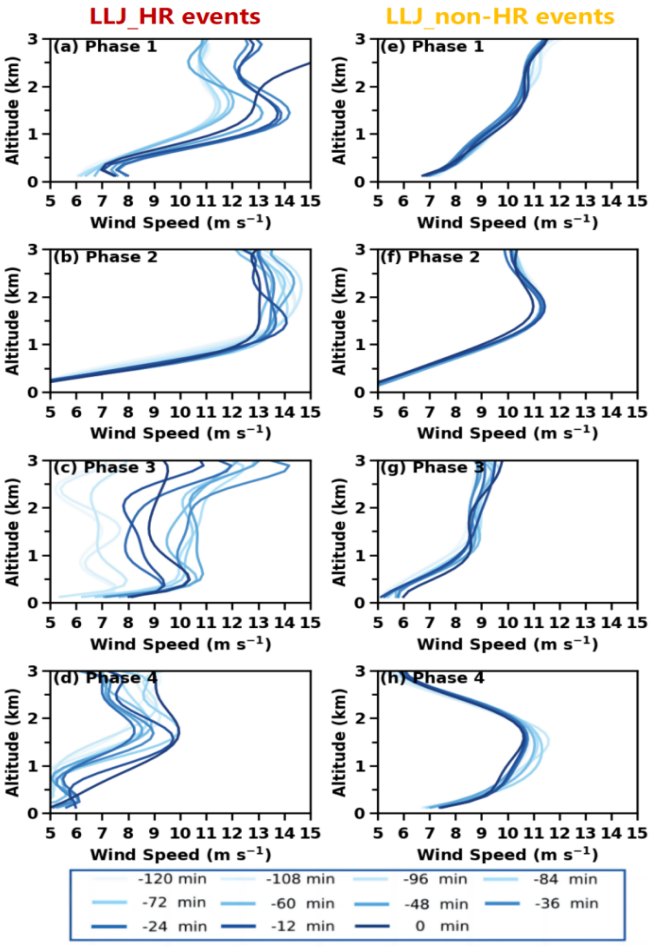

Figure S3. Same as Figure S2, but for HR events (≥ 95th percentile).

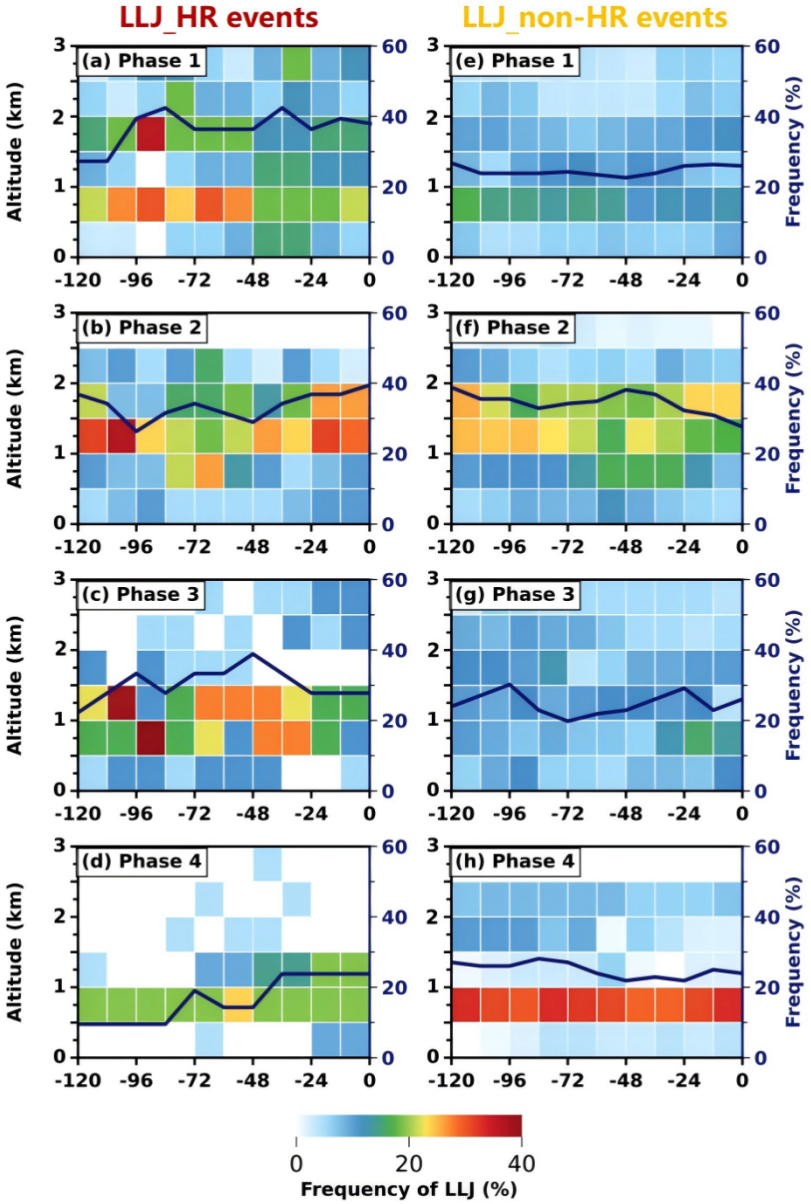

Figure S4. Time-height evolution of LLJ occurrence frequency (color shading, every 12 min, within 500 m vertical bins) detected by RWP with 2 hours preceding nocturnal rainfall in LLJ-HR (≥85th percentile) events in (a) ROI-1 during Phase 1, (b) ROI-2 during Phase 2, (c) ROI-3 during Phase 3, and (d) in ROI-4 during Phase 4. Dark blue solid lines denote accumulated LLJ frequency over 0–3 km latitude. (e-h) Same as (a-d), but for LLJ_non-HR events

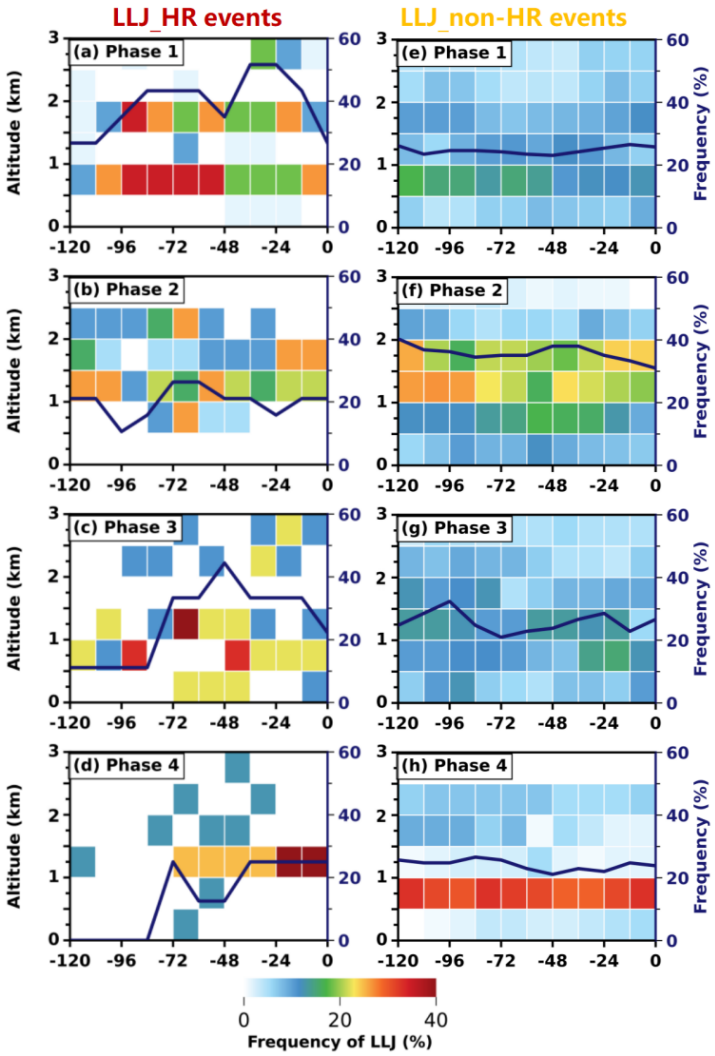

Figure S5. Same as Figure S4, but for HR events (≥95th percentile).

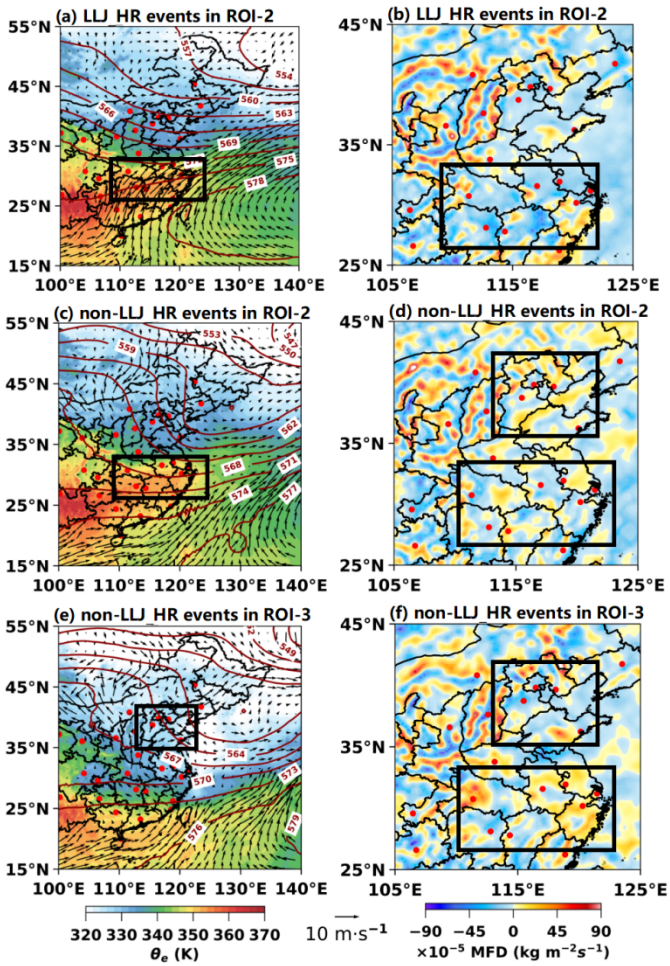

Figure S6. Distributions of (a) equivalent potential temperature (shading, unit: K) at 850 hPa, superimposed with 850 hPa horizontal wind vectors (black arrows) and 500 hPa geopotential height contours (red solid lines) and (b) the integrated moisture flux divergence (shading, unit: kg · m^{-2} s^{-1}) between 1000 – 700 hPa for LLJ-HR events within 1-hour time window preceding nocturnal rainfall onset in ROI-2 during Phase 2. The reference vector (10 m s^{-1}) is shown at the lower corner. (c-d) and (e-f) Same as (a-b), but for LLJ_non-HR events in ROI-2 and LLJ_non-HR events in ROI-3, respectively.

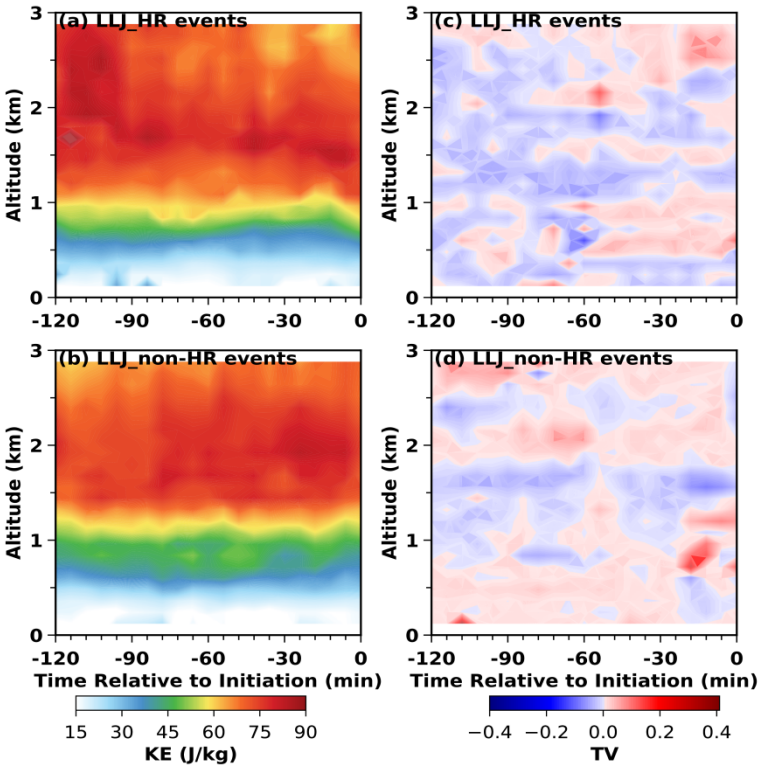

Figure S7. (a) Evolution of mean wind kinetic energy (units: J kg^{-1}) and (c) vertical transport of kinetic energy preceding nocturnal rainfall in ROI-2 during Phase 2 for LLJ_HR events. (b) and (d) Same as panels (a) and (c), but for LLJ_non-HR events.